ELSEVIER

Journal of Structural Geology 29 (2007) 241–255

JOURNAL OF STRUCTURAL GEOLOGY

www.elsevier.com/locate/jsg

Deformation and recrystallization mechanisms in mylonitic shear zones in naturally deformed extrusive Eocene–Oligocene rocksalt from Eyvanekey plateau and Garmsar hills (central Iran)

Zsolt Schléder*, János L. Urai

Geologie-Endogene Dynamik, RWTH Aachen, Lochnerstrasse 4-20, 52056 Aachen, Germany

Received 9 February 2006; received in revised form 28 July 2006; accepted 9 August 2006
Available online 9 November 2006

Abstract

Microstructural processes in mylonitic shear zones from extrusions of Eocene–Oligocene rocksalts from Garmsar hills and Eyvanekey plateau (central Iran) are described and analyzed. The halite samples were studied by transmitted light microscopy of gamma-irradiated thin sections, subgrain size palaeopiezometry of polished and chemically etched samples and texture measurements by electron backscatter diffraction (EBSD).

The studied shear zones are thin (<5 cm), subhorizontal and bedding parallel. The protomylonite comprises 2–6 mm sized grains, occasionally rich in primary fluid inclusions indicative of their primary non-recrystallized state. Abundant, well-developed subgrains suggest that the protomylonite was deformed mainly by dislocation processes. Elongated subgrains at grain edges point to recrystallization by fluid-assisted grain boundary migration. Recrystallized, strain-free grains are common. The material in the mylonitic zones is fine grained (~0.6 mm) with strong shape-preferred orientation. Microstructures such as oriented fibrous overgrowths and growth banding (observed in gamma-irradiated sections) suggest that the principal deformation mechanism was solution-precipitation creep (non-conservative grain boundary migration and grain boundary sliding accommodated by solution-precipitation). Crystal fabrics measured by EBSD show a weak crystallographic preferred orientation that is consistent with solution-precipitation accommodated grain boundary sliding.

Using published flow laws, the strain rate in the fine-grained mylonites is about 10^{-10} l/s, which is in a good agreement with earlier in situ measurements on glacier salt flow rate.

Keywords: Rocksalt; Salt glacier; Halite mylonite; Shear zone; Deformation mechanism; Solution-precipitation creep

1. Introduction

Over the past 50 years our understanding of the salt-sediment system has increased tremendously. Aspects of the dynamics of salt tectonics and sealing of fluids are quantified, but many questions are unresolved to date (Jackson, 1995). Salt is also useful as analogue material for understanding the microstructural processes and textural development in silicate rocks (Drury and Urai, 1990).

An interesting, yet poorly understood phenomenon is the extraordinary mobility of glacier salt that flows downhill at geologically high strain rates at very low shear stress in the Zagros Mountains and in central Iran (Talbot, 1979, 1981, 1998; Talbot and Rogers, 1980; Talbot and Jarvis, 1984; Talbot et al., 2000; Talbot and Aftabi, 2004). Recognition of equivalents of these salt glaciers was documented by studies of the Gulf of Mexico salt province (Fletcher et al., 1995), where the extruded salt flows on the sea floor under a thin, unconsolidated layer of sediment. Besides the recent examples,

* Corresponding author. Present address: Midland Valley Exploration Ltd., 144 West George Street, Glasgow G2 2HG, UK. Tel.: +44 141 332 2681; fax: +44 141 332 6792.
E-mail address: zsolt@mve.com (Z. Schléder).

0191-8141/$ - see front matter © 2006 Elsevier Ltd. All rights reserved.
doi:10.1016/j.jsg.2006.08.014

salt glaciers were shown to have been present in many salt bearing sedimentary basins during their geologic evolution (Volozh et al., 2003; Mohr et al., 2005).

If glacier salt had the well known rheology of domal salt (Wawersik and Zeuch, 1986; Carter et al., 1993; Ter Heege et al., 2005b), the salt glaciers would be far too strong to flow under their own weight. Solution-precipitation creep was inferred to account for the unusual weakening of glacier salt (Wenkert, 1979). The model explains fairly well the observed shear stress and strain rate (<0.25 MPa, 1.1×10^{-11} to 1.9×10^{-9} l/s; Jackson, 1985) in salt glaciers as creep due to diffusion of ions through an interstitial salt-brine solution. This weak behavior was also observed in experimentally deformed fine-grained wet salt (with water content about 0.05 wt%) by Urai et al. (1986), and extensive work by others (Spiers et al., 1990; Lohkämper et al., 2003) has clarified many details of this process.

The average grain size in domal salt is around 5–30 mm (Warren, 2006). Solution-precipitation creep is dominant over dislocation creep in fine-grained wet salt. From Kuh-e-Namak (Dashti, Iran) salt glacier, Talbot (1981) reported processes of progressive subgrain rotation and tensional failure on cleavage planes which resulted in grain size reduction. He also proposed that fluid-assisted grain boundary migration is important both in domes and glaciers. By studying one sample of naturally deformed glacier salt from Iran, Urai et al. (1986) noted that the halite grains do not contain any substructure but do show the same microstructural features as seen in the fine-grained, synthetic wet halite deformed under wet conditions.

The aim of this study is to extend our understanding of deformation and recrystallization mechanisms in halite (Urai et al., 1986, 1987; Wawersik and Zeuch, 1986; Spiers et al., 1990; Senseny et al., 1992; Carter et al., 1993; Peach et al., 2001; Watanabe and Peach, 2002; Hunsche et al., 2003; Ter Heege et al., 2005a,b; Pennock et al., 2005) to processes in glacier salt. The samples analyzed in this study are from the Garmsar hills and Eyvanekey Plateau (central Iran), where the Eocene–Oligocene salt was squeezed out under the thin cover of Alborz mountains.

2. Salt extrusions in central Iran

2.1. Lithostratigraphy in the Great Kavir and in its sub-basins

In central Iran Tertiary, salt reaches the surface in many places. The most voluminous salt outcrops can be found in the Great Kavir basin and in its peripheral sub-basins (Qom, Garmsar and Damghan basins) (Fig. 1). The Tertiary, which lies unconformably on folded Mesozoic strata, starts with marine, Eocene sediments, associated with volcanic rocks (Jackson et al., 1990).

The first evaporites (~500 m thick) were deposited during the middle Eocene in the southern part of the Great Kavir basin. Due to regression towards the end of Eocene, deposition of gypsiferous rocksalt started in the northern part of the basin

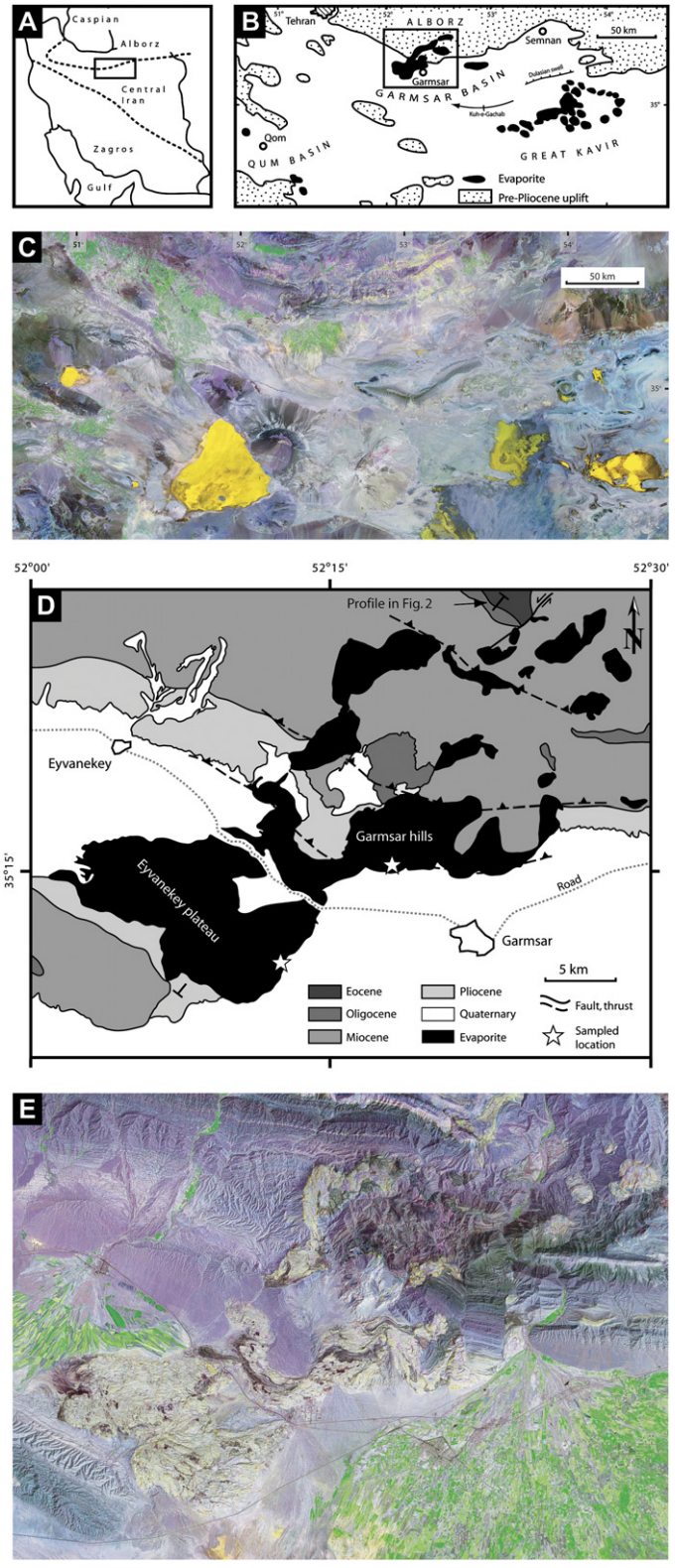

Fig. 1. Simplified regional setting of Garmsar hills, Eyvanekey plateau and surroundings. (A) Location in the map of Iran. (B) Evaporites on the surface in the Garmsar basin and adjoining Qom and Great Kavir basins (after Jackson et al., 1990; Talbot and Aftabi, 2004). (C) GeoCover landsat image corresponding to cartoon (B). (D) Simplified geological setting of Garmsar hills and Eyvanekey plateau after geological map of Amini and Rashid (2005). (E) GeoCover landsat image corresponding to area of map D (source: https://zulu.ssc.nasa.gov/mrsid/).

(Qom and Garmsar). The deposition of these evaporites lasted until the latest Eocene–early Oligocene (Fig. 2A) leading to the accumulation of a few hundred meter thick evaporite sequence (Jackson et al., 1990).

During late Eocene tectonic movements, the sub-basins became separated from the Great Kavir basin. After these tectonic movements a new sedimentary cycle started, the base of which is marked by a distinct unconformity. This new cycle started with red continental clastics and Oligocene evaporites (Lower Red Formation, LRF), which are overlain by an upper Oligocene–lower Miocene marine unit, the Qom formation, in turn overlain by the Miocene Upper Red Formation (URF) (Jackson et al., 1990; Talbot and Aftabi, 2004). The LRF reaches its maximum thickness of ~1000 m south of the Qom basin and consists mainly of red sediments intercalated with volcanics. Evaporites of the LRF are ~300 m thick in the Qom basin, further east the beds change to nonevaporitic clastic facies (Jackson et al., 1990). The Qom formation is a 1000 m thick sequence of platform-type limestone, marl shale, sandstone and gyprock (Gansser, 1960a; Gretener, 1982; Jackson et al., 1990). The Miocene URF reaches the maximum thickness of ~5000 m in the Qom and the Garmsar basins. The URF can be divided into a lower evaporitic and an upper sandy part in the Qom basin, while in the Garmsar basin it can be subdivided into three members (Jackson et al., 1990). The lowermost member (~700 m) consists of a rhythmic saline facies with thin (<10 m) impure rocksalt beds. The middle member (~3000 m) is gypsiferous mudrock, the uppermost member is composed of cyclic saline mudrock gyprock alterations (Fig. 2A). However, a fully reliable stratigraphic subdivision of the URF in the Great Kavir is hampered by the lack of paleontologic and subsurface data and the dominance of monotonous mudrocks (Jackson et al., 1990).

Several authors (Gansser, 1960b; Jackson et al., 1990; Talbot and Aftabi, 2004) proposed that all the salt structures in central Iran involve the same two salt sequences: a relatively pure, upper Eocene–lower Oligocene salt (base of lower Oligocene Lower Red Formation) and a variegated, impure lower Miocene salt sequence (lower Miocene Upper Red Formation).

2.2. Geological setting of Eyvanekey plateau and Garmsar hills

The Garmsar basin (Figs. 1 and 2) is a peripheral embayment of the Tertiary Great Kavir basin, separated by the Kuh-e-Gachab and Dulasian swell. The Tertiary depocenter in the Garmsar Basin is situated roughly between the cities of Eyvanekey and Garmsar. As the stratigraphy is strongly distorted by salt tectonics, their exact thickness is not resolved, but proposed to exceed 8000 m in this foredeep (Jackson et al., 1990).

The Tertiary salt was extruded under the thin cover of Alborz mountains and reached the surface north of Garmsar and was further squeezed to south producing a 20 × 10 × 0.2 km Eyvanekey plateau salt sheet (Figs. 1 and 2B) (Talbot, pers. comm.; Talbot, in preparation). The Eyvanekey plateau and the Garmsar hills consist predominantly of large diapiric masses of salt and gyprock with inclusions of mafic volcanic rocks with subordinate marl, calcareous marl, shale and sandstone (Amini and Rashid, 2005). Owing to the lack of fossils,

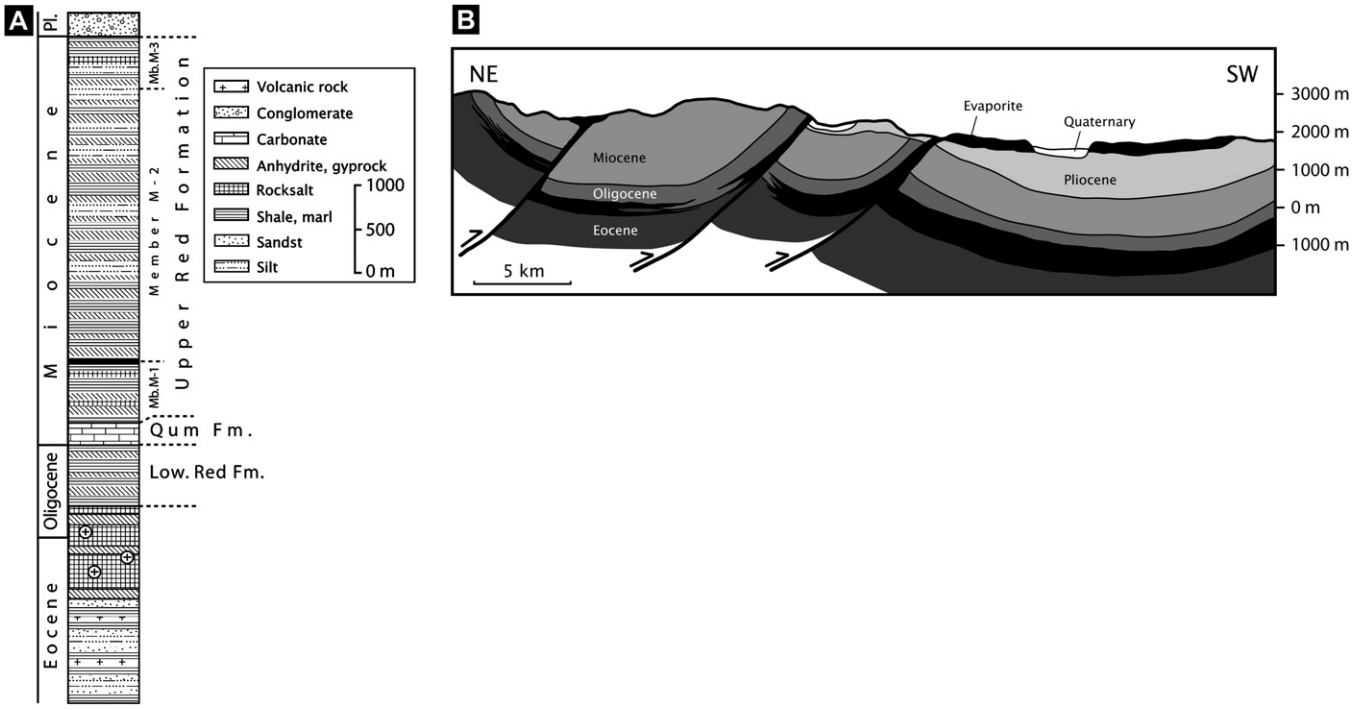

Fig. 2. (A) Lithostratigraphical column of the Garmsar basin after Jackson et al. (1990). The Eocene–Oligocene rocksalt is the main source for the extrusions of Garmsar hills and Eyvanekey plateau. (B) Cross-section through the Garmsar hills and Eyvanekey plateau (modified after Amini and Rashid, 2005). For the position of the profile see Fig. 1D. Vertical exaggeration is about twofold.

the exact age of the evaporitic mass cannot be determined although based on lithologic similarities to Qom Kuh and the Great Kavir diapirs (Talbot and Aftabi, 2004), it is very likely that both the hills and the plateau are made up of evaporites both of upper Eocene and Oligocene age. It is also unknown whether the salt sheet is still moving today (Talbot, pers. comm.).

The present surface of the evaporite extrusion in the plateau and hills is covered predominantly with light green to pale brown gypsite with subordinate marl and calcareous marl (Amini and Rashid, 2005). Rocksalt outcrops are rare, but halite is accessible in the numerous open-pit and underground salt mines that were opened in the last 10 years (Talbot, in preparation).

Although in both locations the salt is strongly deformed by sets of recumbent folds, the bedding is generally subhorizontal. Commonly the salt mass contains thin layers of halite with strong shape-preferred orientation: halite mylonites.

2.3. Samples

In this study we report detailed microstructural analysis of mylonitic halite samples from two, currently abandoned, open-pit salt quarries (Fig. 1D). One sample was collected at the southern edge of the Garmsar hills (co-ordinate: 35°16′N; 52°17′E, sample referred to as "GH" hereinafter). This sample comprises a few, <1 cm thin mylonitic zones and protomylonites (Fig. 4A). In the whole outcrop, the mylonitic zones are commonly less than 5 cm thick, and develop parallel to the bedding at the bottom of the individual beds (Fig. 3). In outcrop, the salt is horizontally bedded, with beds of about 20 cm thick, which often show gradual colour change of grayish white to white and slight grain size change from finer at the bottom and coarse grains at the top (Fig. 3). We interpret this variation in individual beds to reflect the variations in sedimentary conditions. Abundant primary features (see below) in the non-recrystallized grains imply that the salt is not completely recrystallized.

We note that the similar-looking beds in the outcrop may represent only one or two beds, which were isoclinally folded – although the hinges of these were not found in our outcrops. Such bedding-parallel shear zones were also observed by Talbot (1981) in the Kuh-e-Namak salt glacier, suggesting that they are fairly common in extrusive salts.

The other sample was collected at the eastern edge of the Eyvanekey plateau (co-ordinate: 35°12′N; 52°12′E, sample referred to as "EP" hereinafter). This sample is about 5 cm thick and consists of mylonitic salt with strong shape-preferred orientation (Fig. 4B).

3. Methods of study

Samples were cut parallel to the lineation and perpendicular to the foliation using a diamond saw with a small amount of water to prevent microcracking (Schléder and Urai, 2005). After this, the samples were decorated by gamma-irradiation in the Research Reactor of Forschungszentrum Jülich using a technique similar to that of Urai et al. (1985). The irradiation was done in a purpose-built heated container at a constant temperature of 100 °C. The dose rate was between 4 kGy/h and 6 kGy/h and the total dose was about 4 MGy. The colour intensity developed in the samples during gamma-irradiation reflects the heterogeneous distribution of solid solution impurities and crystal defects in halite grains (Murata and Smith, 1946; Przibram, 1954; van Opbroek and den Hartog, 1985; Urai et al., 1985; Garcia Celma and Donker, 1996).

Thin sections were prepared following the procedure of Spiers et al. (1986), Urai et al. (1987) and Schléder and Urai (2005). Thus, the samples were mechanically ground and polished dry on grinding paper, etched in 5% undersaturated NaCl solution for 10 s, subsequently rinsed for 3 s with a strong jet of *n*-hexane and finally dried in a jet of warm air. This sample preparation removed surface scratches and revealed dislocation substructure. The thin sections were studied with reflected and transmitted, plane-polarized light microscopy.

To attempt to reveal variation in trace element content in selected grains, conventional microprobe analyses (Type: JEOL JXA-8900R) were carried out at the RWTH Aachen.

On the EP sample, crystallographic orientation data were acquired from EBSD patterns using a JEOL 6100 (at the RWTH Aachen), typically operating with acceleration voltage of 20 kV and beam current of 8 nA. The EBSD patterns were indexed with the CHANNEL 5 software (HKL Technologies) using the file for halite consisting of 46 lattice planes.

Multiple beam maps (12 horizontal × 4 vertical) were used to map the specimen. For an individual map, data points were collected on an orthogonal grid of 106 × 73 at a fixed step size of 40 μm by moving the sample and keeping the beam stationary. After the mapping, the individual maps were stitched together using the CHANNEL 5 software. Misorientation between two stitched maps is <3°, and is due to the gradual orientation error in each individual map. Misorientation data between individual grains were calculated separately for each map and these data were used for the misorientation distribution histogram. The quality of the EBSD data is very good – the fraction of patterns that could no be indexed was below 10% – with the exception of the immediate vicinity of the margins of individual maps, where typically 1–2 pixels could not be indexed. The maps were further processed in order to remove erroneous data and to provide more complete reconstruction of the microstructure (Prior et al., 2002; Bestmann and Prior, 2003). The accuracy of individual measurement is better than 1°. The misorientation angle between two grains was calculated by selecting the minimum misorientation angle from all possible symmetric variants (Wheeler et al., 2001).

4. Results

4.1. Observations on microstructure and texture measurement

Both samples studied in this paper are almost pure halite (~98%) with polyhalite, anhydrite and limestone fragments as main impurity phase. The GH sample contains a few thin

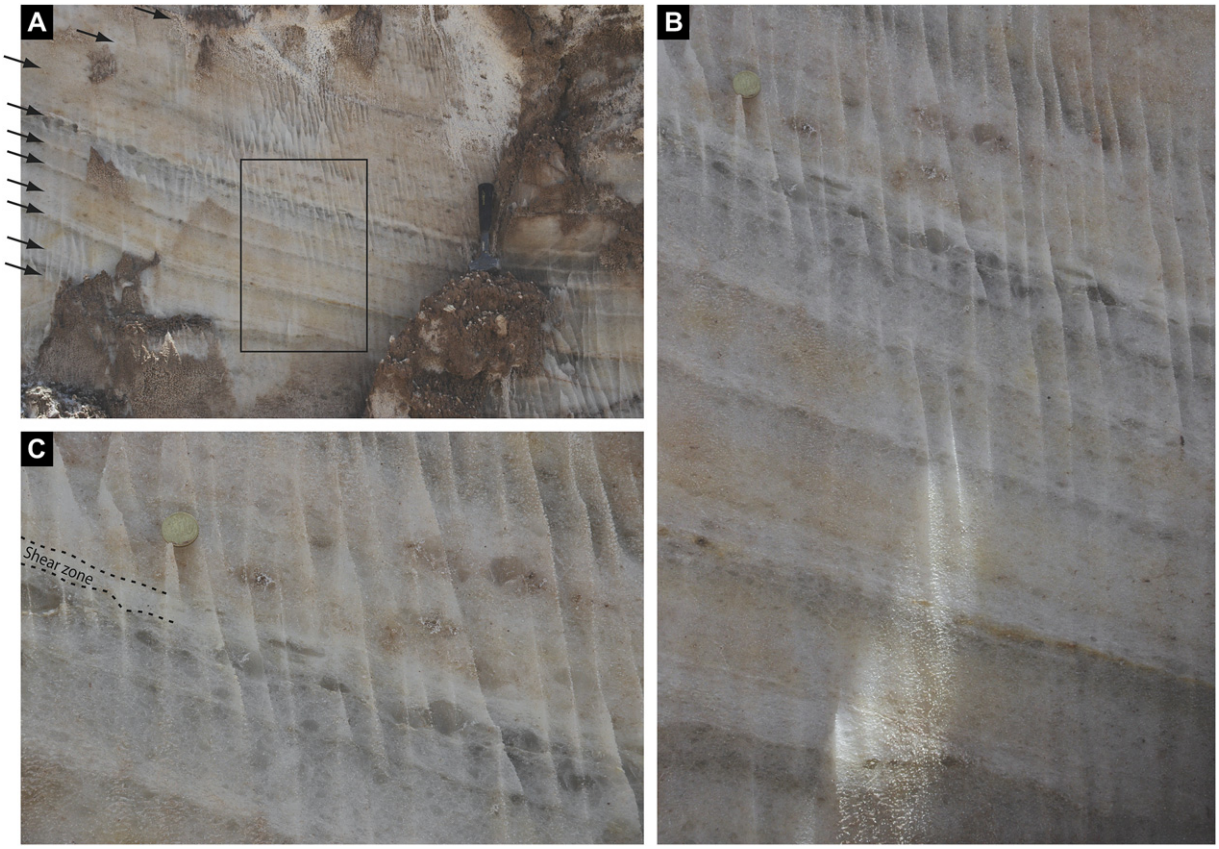

Fig. 3. (A) Bedding-parallel mylonitic zones in a salt wall (looking E) exposed near the abandoned salt mines in the Garmsar hills. The strata dip 10° to SW. The mylonitic zones are relatively thin (<3 cm, see arrows) and are characterized by strong shape-preferred orientation and small grain size. The position of the B image is indicated with the rectangle. Hammer for scale. (B) Detail of the image (A). Note that the shear zones occur often above coarse-grained, dark gray coloured layers. The vertical fluting is a karstic feature due to rainwater. Coin ($d = 2$ cm) for scale. (C) Detail of image (B). Note the flattened porphyroclast in the shear zone and the abundance of large grains at the bottom of the shear zone.

mylonitic zones and protomylonite, the EP sample is made entirely up of mylonitic material (Fig. 4). In thin section, the mylonites from both locations show comparable microstructures; the descriptions presented here apply to both samples. The transition from coarser grained protomylonite to the fine-grained mylonite is rather sharp, but the interface is quite wavy (Fig. 4A).

4.1.1. Protomylonite

The protomylonite consists of slightly elongated, 2–6 mm large grains. The aspect ratio of the grains is about 1.5–2 with the long axis parallel to the mylonitic zones and bedding (Figs. 4A and 5). This shape-preferred orientation (SPO) forms a weak foliation that is clear in outcrop. Commonly, the foliation is oriented at a few degrees to the bedding.

Inspection of unirradiated thick sections (~1 mm) under plane-polarized transmitted light reveals that some grains contain regions with numerous fluid inclusions (Fig. 5A). The fluid inclusions are smaller than 50 μm and show negative crystal shape. Commonly, the inclusions are arranged into thin, approximately 500 μm wide, parallel bands. The cloudy, fluid-inclusion-rich part of a grain is commonly truncated by the upper and lower neighbour grains, while fluid-inclusion-free, clear halite rims the cloudy part to the directions of the SPO (Fig. 5A and C). Gamma-irradiated sections show white polygonal subgrain boundaries in many grains (Fig. 5C). Subgrains in the grain interiors are equiaxial and have an average size of about 120 μm. In contrast, subgrains close to grain boundaries have an elongated shape, with the elongation parallel to the direction of SPO (Fig. 5C and D). The length of such elongated subgrains can rarely reach 3 mm. In places, two neighbour grains contain such elongated subgrains. In that case, on both sides of the grain boundary which separates those two grains, the elongated subgrains terminate at the grain boundary. Inside the subgrain-poor region and very rarely between the white coloured polygons, a second-order, dark blue coloured, less developed polygonal structure is visible (Fig. 5C). Besides the substructured grains described so far, not uncommonly small, 2–3 mm large grains without any substructure were also noticed (Fig. 5D).

Typically, the grain boundaries have an irregular, lobate morphology with occasional euhedral grain boundary segments. The grain boundaries are invariably filled with connected, lobately shaped fluid and gas inclusions (Fig. 5B). Based on our microstructural observations, connected porosity in our samples is very low.

The etched surface was also studied in plane-polarized reflected light with the aim to verify that all the dislocation structures were decorated by gamma-irradiation (e.g. Fig. 5D). Comparing the transmitted light images and

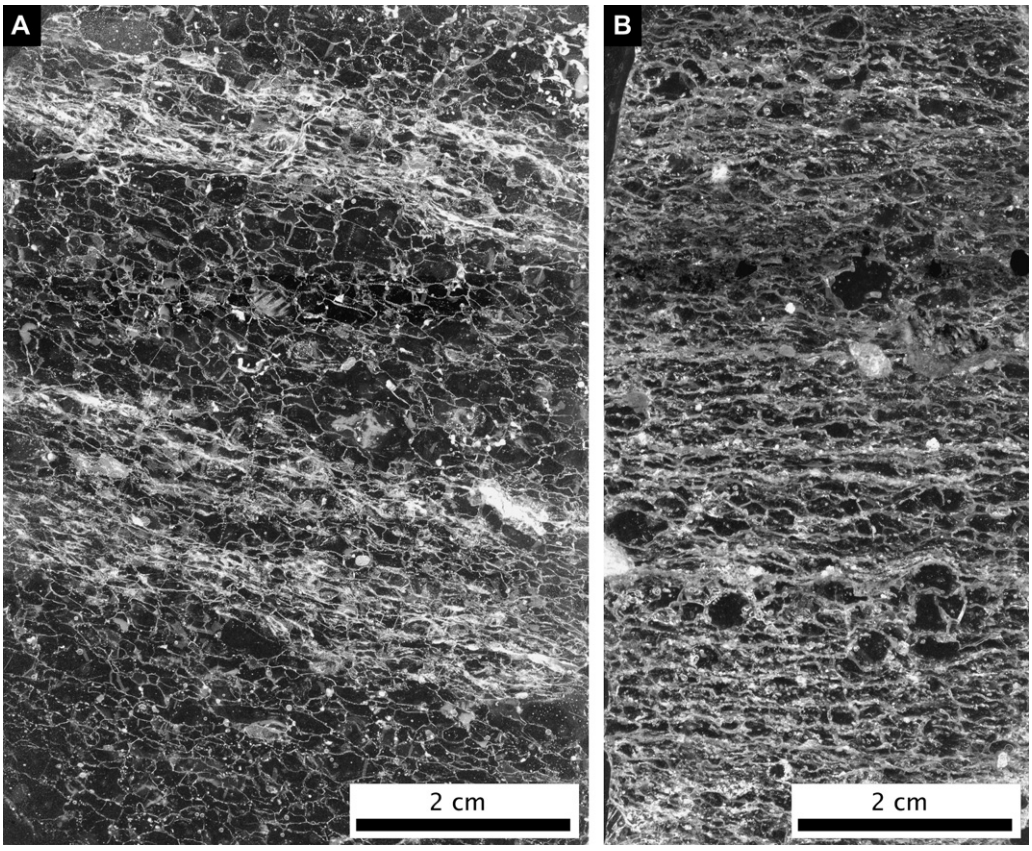

Fig. 4. Dark-field image of scanned thin sections of the samples studied. The grain boundaries and secondary phases show up as light lines and patches, the halite grains occur as dark areas. The Garmsar hill sample (A) contains a few shear zones, the Eyvanekey plateau sample (B) is entirely made up of mylonitic material.

the corresponding reflected light images shows that all the subgrains occurring as white polygons were also visible on the etched surface. In contrast, the second-order polygonal, dark-blue structure within subgrain-poor regions were not visible on the surface.

Secondary phases were found frequently in the protomylonite. Commonly, these are 1–2 mm sized anhydrite crystals or occasional 1–3 mm large limestone fragments. The secondary phases are located commonly at the grain boundaries and more rarely inside the grains, mostly in thin curved bands.

4.1.2. Mylonite

The mylonitic material has a strong shape-preferred orientation and foliation (Fig. 4B). In plane-polarized light of unirradiated samples, the foliation is characterized by numerous impurity phases, such as anhydrite, polyhalite and some limestone fragments arranged into bands. The bands are thin (~1 mm), bedding parallel and have a more or less uniform spacing of about 5 mm. The halite grain size is about 0.6 mm on average, with a few large grains. Some of these large grains contain fluid inclusions identical to those in the protomylonite.

Inspection of etched surfaces in reflected light shows that the vast majority of the small grains lack substructure (Fig. 6A and C), while the sporadic large ones contain well developed subgrains. In transmitted light, irregularly shaped, relatively large inclusions which appear dark grey or black can be observed, mostly on the triple junctions, less frequently on grain boundaries and very rarely inside a single grain (Fig. 6C and D). These inclusions tend to enlarge during dissolution of the sample, indicating a gas at slightly higher-than-atmospheric pressure. The grain boundary structure is similar to that in the protomylonite and contains amoeboid, interconnected brine inclusions (Fig. 6B).

The inspection of gamma-irradiated mylonite in transmitted light reveals more microstructures not seen in the unirradiated sample (Fig. 6E–J). Large grains contain a set of fine, parallel bands. The orientation of these sets is crystallographically controlled and is parallel to (100) as shown by the orientation the cube fluid inclusions in the grains. In the fine grains, a core and mantle structure is commonly observed with dark blue core and pale blue rim. Also in the fine-grained part, in some cases, dark bands are present which are oriented parallel with the grain boundaries (Fig. 6H). Intragranular, highly elongated fibre-like microstructures (~100–200 μm long fibres) around limestone fragments are common (Fig. 6E and F). Invariably, the fibers are parallel to the foliation. Such fibers are not exclusively present around limestone and anhydrite fragments, but also at halite–halite contacts, and in places completely enclosed inside single halite grains (Fig. 6J). In these cases, they form a core–mantle structure with the fibrous microstructures inside the grain (core) rimmed by non-fibrous material (mantle). This mantle commonly shows banding parallel to the grain boundaries (Fig. 6H and J). Inspection of such fibrous structures in reflected light on etched surfaces

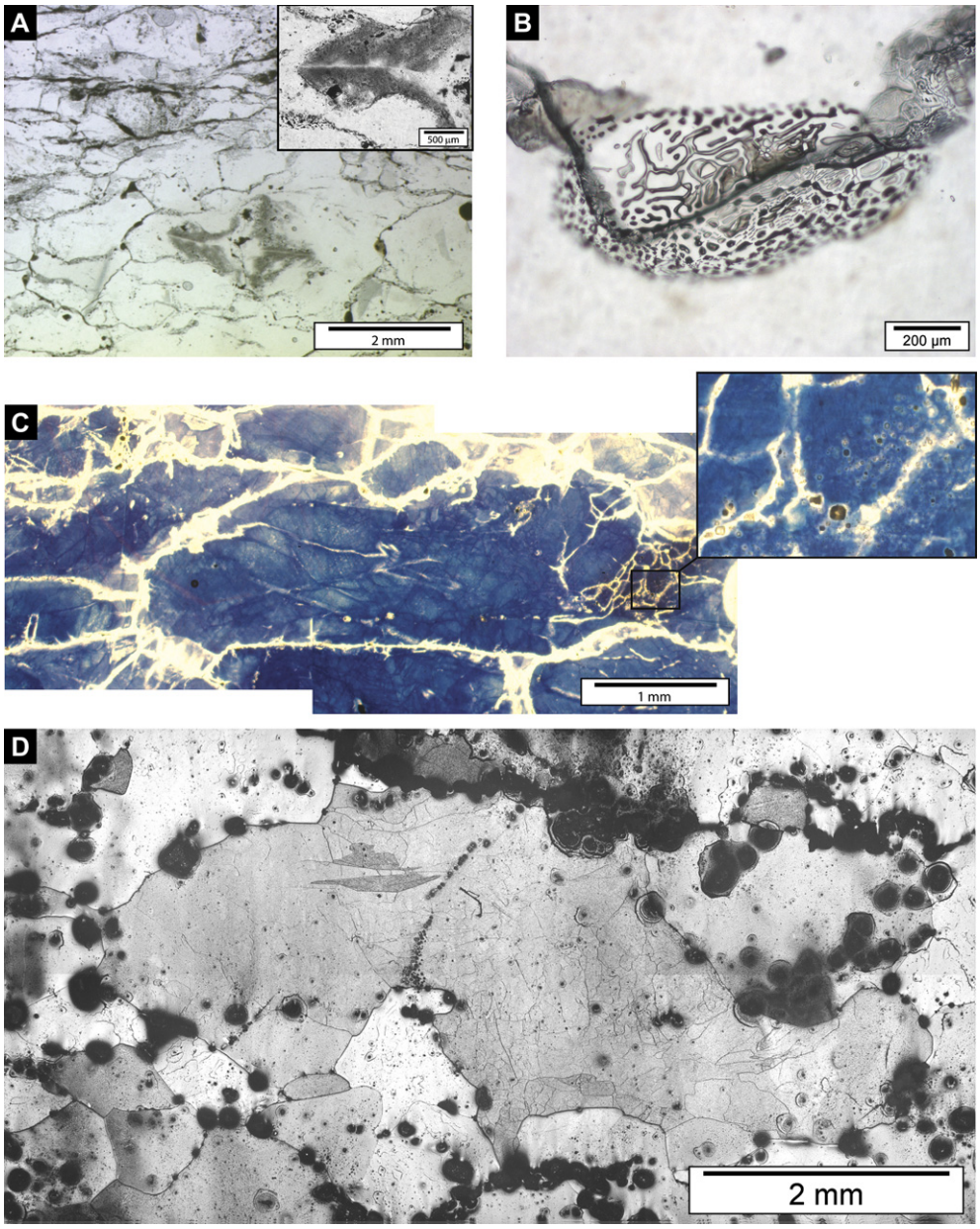

Fig. 5. Micrographs illustrate the characteristic microstructures observed in the protomylonite (sample GH). (A) Plane-polarized, transmitted light image in which the grain boundaries show up as dark lines, the secondary phases as dark patches. The image shows slight shape-preferred orientation and secondary phases inside of grains and at the grain boundaries. Insert: Detail of a fluid-inclusion-rich grain. (B) Grain boundary structure, which shows interconnected, channel-like and separated, island-like fluid inclusions. Some of them opened during sample preparation and are filled with air, thus show up as brown coloured. (C) Highly elongated grain with well-developed subgrains and fluid inclusions (see detail image) on the right and elongated subgrains on the left. Plane-polarized, transmitted light image of gamma-irradiated thin section. Our interpretation is that the once presumably equiaxed grain deformed with dislocation processes, as evidenced by the subgrains, after which recrystallization of fluid-assisted GBM took place, which resulted in an elongated shape. (D) Plane-polarized reflected light image shows a large, elongated grain with well-developed subgrains inside the grain and elongated subgrains at the grain edges. The grain boundaries show up as dark lines. The black spots at the grain boundaries and inside of the substructured grain are fluid inclusions, which opened during sample preparation. The elongated subgrain boundaries at the grain edges point to recrystallization mechanism of fluid-assisted GBM.

reveals that these fibres are not individual grains, but that they are sometimes separated by subgrain boundaries or, more commonly, that no boundary at all is visible between two fibres in reflected light.

4.1.2.1. Crystallographic orientations in the mylonite. Full crystallographic orientation of ~500 grains was measured in sample EP using EBSD. In Fig. 7A and B, crystallographic orientation of individual grains (colour coded according to the crystallographic orientation) together with the corresponding gamma-irradiated thin section is shown. The relatively large grains, seen in the Fig. 7B are remnants of deformed porphyroclasts and occasionally contain primary fluid inclusions. The EBSD measurements confirm the microscope observation, that these grains are typically lack substructure. Fig. 7C shows the corresponding pole orientations for the whole dataset. The

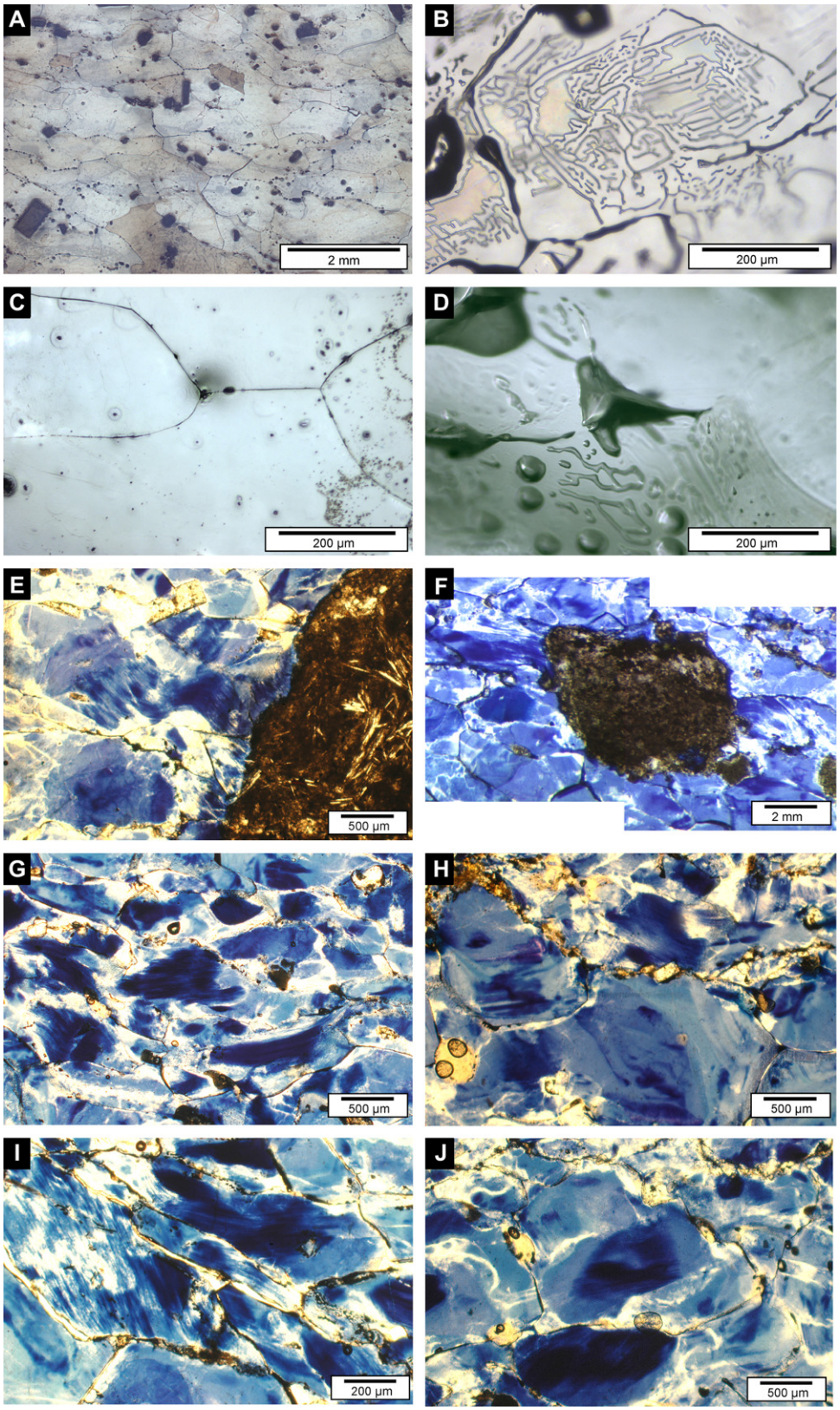

Fig. 6. Micrographs illustrate the characteristic microstructures observed in the mylonite. (A) Plane-polarized reflected light image shows straight to gently curved grain boundaries. Black spots at the grain boundaries and in the grains are either secondary phases or fluid inclusions which opened up during sample preparation. Note that the grains are substructure free. (B) Interconnected fluid inclusions at the grain boundaries. Note also the subcontinuous fluid-filled tubes at the triple junctions. Plane-polarized, transmitted light image. (C) Plane-polarized, reflected light image shows four grains separated by grain boundaries. Note the lack of substructures. (D) The same area in transmitted light (focused deeper than image C) shows relatively large gas (vapour?) inclusions at the grain boundaries and triple junctions. (E and F) Fibrous structure around a limestone fragment. Plane-polarized transmitted light image of gamma-irradiated section. These

fabric is close to random, with a very weak CPO. The few local maxima correspond to the large porphyroclasts. The grain size for the whole dataset was calculated based on the EBSD measurement. The grain size distribution is close to lognormal (Fig. 7D) with the arithmetic mean value around 0.6 mm. Minimum misorientation angle distribution for the complete dataset – depicted on Fig. 7E – shows that low angle misorientations are absent with the most common misorientation at 45°. The presence of that peak may be an artefact and may also relate to the presence of some relative large, 1–4 mm sized porphyroclast relicts embedded in the fine-grained material.

5. Discussion

In most existing reports on deformation experiments on non-porous natural and synthetic rocksalts, the steady-state creep behavior is controlled by dislocation mechanisms and solution-precipitation. In steady state creep, the grain size organizes itself into the boundary of grain size sensitive and grain size insensitive processes (de Bresser et al., 2001; Ter Heege et al., 2005a).

Experimental conditions range in temperature between 20 °C and 250 °C, strain rate 10^{-4}–10^{-9} l/s and confining pressure is up to 70 MPa. Before the onset of recrystallization, in coarse-grained salt the main deformation mechanism is dislocation creep, with the rate controlling mechanism of cross-slip of screw dislocations at high stresses of ~15 MPa and with rate controlling mechanism of dislocation climb at low stresses (5–15 MPa) (Carter and Hansen, 1983; Wawersik and Zeuch, 1986; Horseman and Handin, 1990; Horseman et al., 1992; Carter et al., 1993). Both mechanisms have their own characteristic microstructure: cross-slip produces wavy slip bands, while climb produces equiaxial subgrains. In addition at sufficiently fine-grain sizes (~500 μm) in wet salt solution-precipitation creep can control the rheology (Urai et al., 1986; Peach et al., 2001; Ter Heege et al., 2005b). Dislocation processes and solution-precipitation process act in parallel (e.g. Spiers and Carter, 1998). In the regime, where dislocation creep controls the rheology, the trace amount of brine also plays an important role, as it drastically increases the grain boundary mobility and induces dynamic recrystallization by fluid-assisted grain-boundary migration (e.g. Watanabe and Peach, 2002).

5.1. Inferred deformation and recrystallization mechanisms based on the observed microstructures

5.1.1. Protomylonite

Before attempting to interpret the deformation-related microstructures and to evaluate the possible microstructural evolution of the samples, we first have to be able to unambiguously identify the primary, synsedimentary microstructures. There is a considerable amount of evidence in the literature that cubic fluid inclusions, arranged into bands parallel to (100), are entrapped when rocksalt is deposited in shallow water environment (see Warren, 2006 and references therein). As the halite deforms, grain boundary migration recrystallization removes those inclusions as the migrating boundary sweeps through them (Roedder, 1984; Schléder and Urai, 2005). One might use the presence of fluid inclusions as a criterion to distinguish between recrystallized and unrecrystallized parts. It has to be noted, however, that even in a shallow water environment not all the primary grains are necessarily rich in fluid inclusions (Shearman, 1970; Lowenstein and Hardie, 1985) or, additionally, the primary fluid inclusions may vary in a single grain, e.g. commonly there is a difference in the abundance of inclusions in salt that crystallized near the cube edge compared with that from the centers of the cube faces (Roedder, 1984). Thus, this microstructure gives only a lower bound of the amount of primary grains or, alternatively, upper bound of the amount of recrystallization. In this paper we interpret the fluid-inclusion-rich part of a grain as primary (e.g. Fig. 5A and C), and the origin of the fluid-inclusion-free regions as uncertain, unless other microstructures such as elongated subgrains point to recrystallization (e.g. Fig. 5C and D).

Well developed, equidimensional subgrains in the fluid-inclusion-rich part of the grains (Fig. 5C) point to dislocation processes, and were presumably produced during recovery by climb/glide of dislocations (e.g. Carter et al., 1993; Ter Heege et al., 2005b). The fact that the equidimensional subgrains laterally pass into elongated subgrains (Fig. 5C and D), suggests that the subgrain formation was followed by extensive grain boundary migration recrystallization. The elongated subgrains are interpreted to have evolved by edgewise propagation of subgrains behind migrating grain boundaries (Means, 1983; Means and Ree, 1988). The evidences for extensive GBM, in turn, may imply that grain dissection during GBM is also important mechanism in grain size reduction. In the subgrain-poor regions the presence of dark blue, subgrain-like polygonal microstructure (Fig. 5C) which was not etched is interpreted as low-energy subgrain walls, with insufficient amount of dislocations to become subgrains (Humphreys and Hatherly, 1996). If this suggestion is correct, this would indicate that concurrent subgrain formed behind the moving grain boundary during dynamic recrystallization.

In some cases, the elongated subgrains occur at both sides of a grain boundary. Such a microstructure can be explained in two different ways. One explanation is that between the two recent grains there existed one highly deformed grain, which was simultaneously and completely replaced by its two neighbours, resulting in elongated subgrains on both sides.

microstructures are interpreted as strain fringes (Passchier and Trouw, 2005). The black curves are grain boundaries the white particles at the grain boundaries are secondary phases (mainly anhydrite). (G) Fibrous microstructure in the pure halite part. The grain boundaries show up as black curves. Note the widespread presence of the fibrous structures. (H) Dark coloured bands which are parallel to the grain boundaries. These dark bands might be regarded as evidence for non-conservative grain boundary migration. (I) Similar structure to (G). The grain boundaries were slightly opened up during sample preparation. (J) Core–mantle structure with fibrous structure inside the grain completely enclosed by non-fibrous halite.

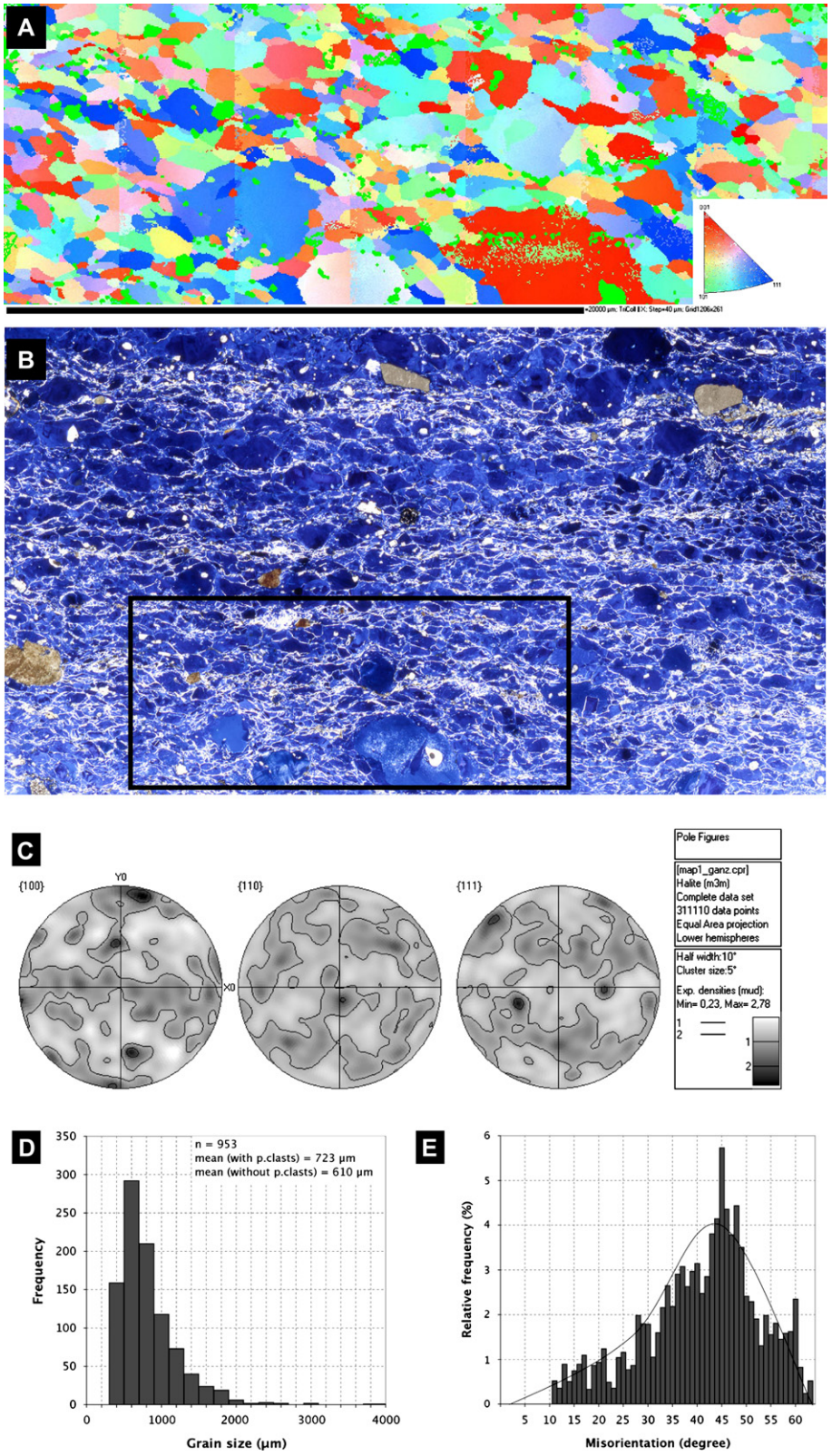

Fig. 7. (A) Part of the automated EBSD map of the EP sample. The map has been coloured according to orientation (green pixels = zero solution), with grain boundaries (>10° misorientation) coloured in black. The area was mapped in 48 maps, with a step size of 40 µm. (B) Microstructures of the thin section, showing the measured area in (A). (C) Equal area, lower hemisphere projections of orientation data. The sample shows a very weak crystallographic preferred orientation. The few local maxima correspond to the orientation data from the large porphyroclasts. (D) Grain size statistics based on the EBSD measurement. The mean grain size is about 0.6 mm. (E) Minimum misorientation angle distribution for all orientation data. The histogram represents neighbour pair misorientation. Solid black line indicates the theoretical misorientation distribution for randomly oriented grains.

Alternatively, this microstructure can be explained with a process somewhat similar to the crack–seal mechanism (Ramsay, 1980), that is the two neighbour grains move away from each other, perhaps with grain boundary sliding/solution-precipitation creep or both, and a gap opens between them which is subsequently sealed with precipitates from the grain boundary fluid. In the latter case, the microstructure points to deformation by grain boundary sliding/solution-precipitation creep as an additional deformation mechanism beside the dislocation processes. It is hard to find unambiguous microstructural evidence for those mechanisms (Passchier and Trouw, 2005).

Equidimensional subgrains do not exclusively occur in the fluid-inclusion-rich part of the grains, but also in the fluid-inclusion-poor part. It can be that this part of a grain is also primary, e.g. it was never swept by a migrating boundary, or, alternatively, it can be that it represents an already recrystallized but subsequently deformed portion of a grain (Schléder and Urai, 2005).

New, substructure free, euhedral grains (Fig. 5D) can be explained by the process of nucleation, in which new grains nucleate at the grain boundary region and grow at the expense of the old, deformed ones. It is unclear whether these grains were nucleated during the upward transport, or are results of late, post-extrusion recrystallization after contact with rainwater. Regardless of their origin these grains are always smaller than the large elongated ones so that the original grain size of the host rock was coarser than that in our samples.

As possible processes for grain size reduction, based on studies of salt glacier in southern Iran, Talbot (1981) proposed processes of subgrain rotation and intergranular cracking of the porphyroclasts, which lead to grain size reduction. We did not find evidence for this in our samples, we note however, that Talbot (1981) studied Hormuz salt from a different setting with a possibly different deformation history (strain rate, differential stress) before and after extrusion. It is also unclear whether the Garmsar prototype microstructures of the protomylonite represent steady state microstructure.

5.1.2. Mylonite

The lack of strong CPO (Fig. 7) and dislocation substructure suggests that the mylonite did not deform by dislocation processes. The large grains in the mylonites with well-developed subgrains, fluid-inclusion bands and with sets of perpendicular dark bands seen in the gamma-irradiated sections indicate that these grains are almost certainly remnants of porphyroclasts. This assumption is in good agreement with experimental deformation on wet, fine-grained halite by Urai et al. (1986) who showed that solution-transfer processes dominate over crystal plastic deformation mechanism in fine-grained halite aggregates deformed at low differential stress.

Fibrous microstructures (Fig. 6E–J) around second-phase fragments and between halite grains point to deformation by grain boundary sliding (GBS). The fibrous structures then fill the voids between grains formed by grain boundary sliding. As the gap between two grains opens up they are continuously sealed by precipitates from the grain boundary fluid (cf. Fig. 1 of Schenk and Urai, 2004). Following this approach, fibrous structures around limestone particles are interpreted as strain fringes around rotating rigid blocks (Fig. 6E and F). Fibrous microstructures, similar to those reported here, were also observed in some other rocks, and are also consistent with grain boundary sliding and solution-precipitation creep (Rutter et al., 1985; Cox and Etheridge, 1989).

The core–mantle structures with the fibrous microstructures inside a single grain, surrounded by non-fibrous material are interpreted as overgrowth structures (Fig. 6G–J) formed by non-conservative grain boundary migration. The growth bands may reflect changes in chemistry of the grain boundary fluid (Murata and Smith, 1946). Alternatively, the growth bands could record stages of grain boundary energy driven grain growth. We have attempted to measure the chemical variation inside such a banded grain using electron microprobe analysis, but results show that the impurity content is below the detection limit (0.02%). The occurrence of dark blue fibrous microstructure may also be due to local enrichment in some chemical elements along the fibre though the exact mechanisms, which are responsible for the development of such microstructure, are not clear.

The presence of voids (Fig. 6C and D), seen now as vapour inclusions, could either be explained by the process of GBS or, alternatively, they may represent dissolution caused by rainwater. As the rainwater dissolves halite from the shear zone, the zone becomes enriched in residual secondary phases. It has been experimentally demonstrated by Hickman and Evans (1991) that such a mixed-phase aggregate is particularly susceptible to pressure solution. The authors reported that a small percentage of secondary minerals – especially clays – dramatically enhances the rate of pressure solution. In the samples analyzed in this paper we did not find clays at the grain boundaries, neither in the wall rock nor in the shear zones, which would suggest that this enhanced pressure solution did not take place, though it may play a role in other extrusive rocksalts as they reportedly contain traces of clay minerals (Talbot and Aftabi, 2004).

5.2. Rheology of the extrusive salts as predicted by the flow laws

The deformation and recrystallization microstructures developed in the protomylonite and mylonite show that the microstructural processes are significantly different between the two rock types. Based on the microstructures we inferred above that the protomylonite presumably deformed mainly by dislocation creep, while the main deformation mechanisms in the mylonitic shear zones are solution-precipitation creep and GBS accommodated by solution-precipitation. In what follows we attempt to quantify the effect of these differences on rheology.

5.2.1. Stress and strain rate calculation

Experimental deformation of various rocks showed that there is a strong correlation between the steady state subgrain size D and flow stress σ (e.g. Twiss, 1977; Carter et al., 1993).

This relationship for halite can be written by (Schléder and Urai, 2005)

$$D\,(\mu m) = 215\,\sigma^{-1.15}(MPa) \quad (1)$$

The relationship can be used for estimating the paleostress in halite. For this calculation we measured the sizes of the equiaxial subgrains by the method of equal circular diameter (ECD), which involves the tracing of subgrain boundaries from digital photos of etched thin sections taken in reflected light, and calculating of the enclosed subgrain area using ImageJ software. The calculated differential stress for the protomylonite is 1.4–2 MPa (95% confidential limits, Table 1), which is in good agreement with the literature data for other rocksalts (Carter et al., 1993). Such high differential stress clearly does not exist in the glacier and we interpret these microstructures to have formed during the upward transport of the salt mass in the extrusion canal. In the glacier itself, the deformation is driven by the downslope component of gravity. The common salt glacier thickness does not exceed 200 m, and with a slope of 5° the shear stress is about 0.4 MPa, (Wenkert, 1979; Jackson, 1985).

It has been proposed that natural rocksalt deforms with a combination of dislocation climb and solution-precipitation creep processes which act in parallel (Spiers and Carter, 1998). The microstructures seen in the protomylonite are in agreement with this assumption, enabling us to calculate the strain rate using the Eq. (2) for dislocation climb and Eq. (3) for solution-precipitation creep. For solution-precipitation creep there are numerous flow law parameters in the literature (Lohkämper et al., 2003). To calculate the strain rate we used the flow law parameters quoted by Spiers et al. (1990). In that work, they calibrated the flow law on the basis of experiments on porous and dense polycrystalline aggregates of synthetic rocksalt.

$$\dot{\varepsilon}_{CL} = 8.1 \times 10^{-5} \exp\left(\frac{-51600\ J\ mol^{-1}}{RT}\right)(\sigma_1 - \sigma_3)^{3.4} \quad (2)$$

after Carter et al. (1993);

$$\dot{\varepsilon}_{PS} = 4.7 \times 10^{-4} \exp\left(\frac{-24530\ J\ mol^{-1}}{RT}\right)(\sigma_1 - \sigma_3)/TD^3 \quad (3)$$

after Spiers et al. (1990); where strain rate ($\dot{\varepsilon}$) is expressed in s^{-1}, the pre-exponential constant is in $MPa^{-n}\,s^{-1}$, apparent activation energy is in $J\,mol^{-1}$, Boltzmann's gas constant (R) is in $J\,mol^{-1}\,K^{-1}$, temperature (T) is in °K, differential stress ($\sigma_1 - \sigma_3$) is in MPa and grain size (D) is in mm. For the calculation we assumed that the salt extrudes from a depth of 1.5 km (Fig. 2), thus we used 40 °C as deformation temperature for the protomylonite. This value is admittedly only a crude estimate, since we do not exactly know at which stage the protomylonite was deformed and what was the real geothermal gradient in the area.

The mylonite microstructures depict deformation mechanisms of solution-precipitation creep and GBS accompanied with solution-precipitation. We postulate that the rate limiting process is the solution-precipitation process, enabling us to describe its rheology by Eq. (3). For the mylonite we assumed that the shear zones developed and the deformation took place on the surface and that the deformation occurred mostly in the rainy, relatively cold seasons (Talbot and Rogers, 1980), thus we used 20 °C. The strain rate calculations for the protomylonite indicate that dislocation creep and solution-precipitation creep contribute approximately equally to the total strain rate (Fig. 8). It has to be noted here that if we calculate only with the grain size of the large, elongated grains, dislocation creep dominates over the solution-precipitation creep.

The strain rate calculated for the mylonite is about one or two orders of magnitude higher at much lower shear stress than in the protomylonite. It shows that this material is much weaker than the coarse grained counterparts. If the rheology is comparable to that observed in experiments of Spiers et al. (1986) and Urai et al. (1986) (Fig. 8), the calculated strain rate also agrees well with field measurements (Talbot and Rogers, 1980; Talbot et al., 2000), and corresponds to glacier flow of ~1 m in 2 years.

5.2.2. Initiation of the shear zone

As we discussed above, the protomylonite suggests dislocation creep at differential stress of 1.4–2 MPa. This deformation mechanism is characteristic for the upward transport of the salt through the cold diapir stem. In the glacier the strain concentrates in multiple, narrow shear zones in which the salt deforms by mechanisms of GBS and solution-precipitation creep (Fig. 8). It follows that there has to be a zone where the two deformation mechanisms switch, i.e. where the deformation changes from a dislocation process controlled one to a GBS + solution-precipitation controlled one. Unfortunately, the limited outcrop did not allow us to locate where the salt is extruded. It is possible that the shear zones were already developed before the salt mass reached the surface, or that the strain was accumulated in shear zones when it was squeezed out and moved to its recent position.

Table 1
Statistics of grain and subgrain size and calculated differential stress, strain rate values

Sample	Mean grain size (mm)	1 SD	Mean subgrain size (μm)	1 SD	Differential stress (MPa)	Assumed deformation temperature (°C)	Strain rate (l/s)[c]
Protomylonite (GH)	4	2	114	71	1.4–2	40	7.2×10^{-12} 1.1×10^{-11}
Mylonite (GH and EP)	0.6[a]	0.35	–	–	~0.4[b]	20	1.2×10^{-10}

[a] The mean grain size in the mylonite was quantified based on EBSD measurements.
[b] Shear stress calculated for 200 m thick salt sequence and 5° slope.
[c] For the protomylonite the total strain rate is a sum of those from Eqs. (2) and (3). For the mylonite the strain rate is calculated using Eq. (3).

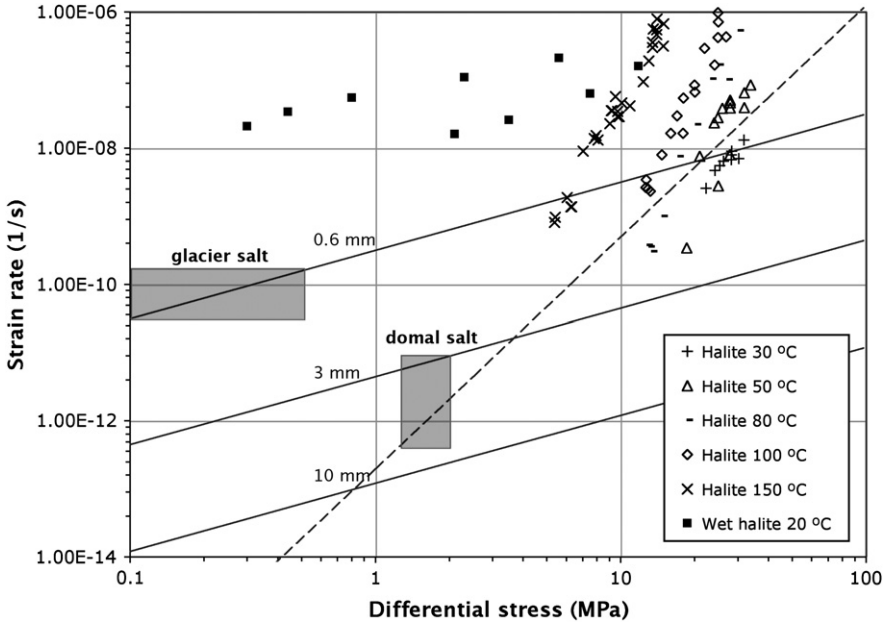

Fig. 8. The diagram shows the calculated differential stress values plotted against the calculated strain rate values for both the protomylonite and mylonite. The differential stress for the protomylonite was calculated using subgrain piezometry (1.4–2 MPa), while the shear stress arising from the downslope component of gravity was taken for the mylonite (<0.4 MPa). For the protomylonite, strain rate was calculated assuming deformation mechanisms of dislocation creep and solution-precipitation creep and that these processes act in parallel (Spiers and Carter, 1998). Thus, the flow law from Carter et al. (1993) is plotted for 40 °C (dashed line) and the flow law for solution-precipitation creep (Spiers et al., 1990) for grain sizes of 3 mm and 10 mm for 40 °C is also shown (solid lines). The strain rate for the mylonite was calculated assuming that the rate controlling mechanism is the solution-precipitation creep. Thus, the flow law of Spiers et al. (1990) was taken and calculated for a grain size of 0.6 mm and a temperature of 20 °C. The relevant field for both domal salt and the glacier salt is indicated with a gray rectangle. Besides these, experimental data from numerous sources (Hansen and Mellegard, 1980; Hansen and Carter, 1984; Handin et al., 1986; Spiers et al., 1986; Senseny, 1988; Horseman and Handin, 1990; Horseman et al., 1992; Hunsche et al., 2003) are also shown for comparison. The grain size in the wet halite test is ~0.1 mm, for the others it is significantly coarser: >5 mm. Note that the experiment on fine-grained wet halite shows a comparable rheology to that calculated for the glacier salt.

Although the protomylonite in the Garmsar hills sample is considerably recrystallized, it is probable that the salt still retained some of its primary grain size variation when it reached the surface. This assumption is supported also by the fact that in the protomylonite primary microstructures such as fluid-inclusion-rich crystals still exist. If the salt retained some slight primary variations in its grain size, this in turn could influence the emplacement of the shear zone in the glacier. As the simplest solution, we suggest this process to be responsible for the emplacement of the bedding-parallel shear zones and that the spacing of the shear zones corresponds to the initial layering produced by primary (synsedimentary) processes (Shearman, 1970; Lowenstein and Hardie, 1985; Warren, 2006). Nevertheless, as the glacier advances downhill, and the whole glacier becomes strongly folded by sets of recumbent folds, resulting probably in that the individual shear zones also become folded.

Mylonitic shear zones illustrated here have never been described in deep salt mines and if they exist they may be quite uncommon indeed, although coarse-grained shear zones do exist during salt diapirism (Kupfer, 1974). Therefore, we prefer the interpretation that such shear zones do not play an important role in deep subsurface halokinetic movement. In the salt extusion perhaps it is the low confining pressure which allows the development of mylonitic shear zones.

5.3. Brine in grain boundaries

Several in situ field measurements showed that the downhill flow of the salt glacier is episodic. Talbot and Rogers (1980) reported accelerated flow after heavy rain, and noted that in dry seasons, the movement involves only daily thermal extension and contraction due to variations in air temperature. There is considerable evidence that these daily variations create an extensive and penetrative crack system (Talbot and Aftabi, 2004), which in turn is able to conduct the rainwater into the salt glacier. The process after which this conducted rainwater wets the whole shear zone is not entirely clear.

The mass transfer, necessary for the solution-precipitation process, could take place in either static fluid network or in migrating fluid. The episodic glacier flow may imply that the mass transport occurred in migrating undersaturated fluids. This assumption seems to be confirmed by the presence of numerous air inclusions at grain boundaries and triple junctions, which could be interpreted as the result of dissolution by the trespassing rainwater.

6. Summary and conclusions

Two mylonitic and protomylonitic samples from naturally deformed extrusive Eocene–Oligocene rocksalt from the

Eyvanekey Plateau and Garmsar hills were studied with the aim to characterize the deformation and recrystallization mechanisms.

1. Conclusions presented in this study may be applicable to other areas where salt glaciers are or were present, since it is very likely, that the deformation involves similar mechanisms in any types of extrusive salts. Mechanics of actively deformed halite at the surface are those of the shear zones described in this paper. Thus, the recent, shallow buried salt glaciers at the Gulf of Mexico may also deform by similar processes and be very weak and many of the ancient now deeply buried bedding-parallel salt flanks (i.e. Christmas-tree structures) were developed by similar processes in weak salt.
2. In the protomylonite dislocation climb controlled creep and solution-precipitation creep were the main deformation mechanisms during the upward transport of the rocksalt. The differential stress was between 1.4 and 2 MPa, as deduced from subgrain size piezometry.
3. As the rocksalt reaches the surface, numerous bedding-parallel shear zones develop, in which the deformation mechanism is solution-precipitation creep (non-conservative grain boundary migration and grain boundary sliding accommodated by solution-precipitation). The microstructural evidences for this are the fibrous structures, growth bands and the lack of crystallographic preferred orientation.
4. The grain size reduction, which is necessary for the grain size sensitive mechanism to become active occurs by nucleation of new grains and/or dissection by grain boundary migration.
5. The formation of the shear zones is perhaps controlled by synsedimentary variation in some mechanical properties, most probably grain size. Thus, the synsedimentary process results in rhythmic variation in grain size, which grain size variation is maintained until the salt reaches the surface. In the salt extrusion, this variation might be the main controlling factor in the emplacement of the shear zone.
6. The GBS and solution-precipitation allow the salt glacier to flow downhill under its own weight with a geologically high strain rate of about 10^{-10} l/s.

Acknowledgements

The authors thank C.J. Talbot for providing sample EP, Dirk Kirch (IMM RWTH Aachen) for the orientation measurements and Manfred Thomé (Forschungszentrum Jülich) for carrying out the gamma irradiation. C.J. Talbot and Abbas Bahroudi are thanked for the introduction into the geology of Garmsar hills and Eyvanekey plateau. We thank the stuff at the Geodynamic Department of Geological Survey of Iran (GSI) in Tehran for the hospitality during the 2005 field season. For helpful discussions O. Schenk, J. Schoenherr, Chris Hilgers at the Department of Geologie-Endogene Dynamik (RWTH Aachen) are acknowledged. The manuscript was improved by thorough reviews of M.P.A. Jackson and W. Schmahl. This work was performed as part project of SPP 1135 (project UR 64/5-1-2) financed by the Deutsche Forschungsgemeinschaft.

References

Amini, B., Rashid, H., 2005. Garmsar geological map 1:100000 in scale. Geological Survey of Iran, Tehran, Iran.

Bestmann, M., Prior, D.J., 2003. Intragranular dynamic recrystallization in naturally deformed calcite marble: diffusion accommodated grain boundary sliding as a result of subgrain rotation recrystallization. Journal of Structural Geology 25, 1597–1613.

Carter, N.L., Handin, J., Russell, J.E., Horseman, S.T., 1993. Rheology of rocksalt. Journal of Structural Geology 15 (9/10), 1257–1271.

Carter, N.L., Hansen, F.D., 1983. Creep of rocksalt. Tectonophysics 92, 275–333.

Cox, S.F., Etheridge, M.A., 1989. Coupled grain-scale dilatancy and mass transfer during deformation at high fluid pressures: examples from Mount Lyell, Tasmania. Journal of Structural Geology 11 (1–2), 147–162.

de Bresser, J.H.P., Ter Heege, J.H., Spiers, C.J., 2001. Grain size reduction by dynamic recrystallization: can it result in major rheological weakening? International Journal of Earth Sciences 90, 28–45.

Drury, M.R., Urai, J.L., 1990. Deformation-related recrystallization processes. Tectonophysics 172, 235–253.

Fletcher, R.C., Hudec, M.R., Watson, I.A., 1995. Salt glacier and composite sediment-salt glacier models for the emplacement and early burial of allochtonous salt sheets. In: Jackson, M.P.A., Roberts, D.G., Snelson, S. (Eds.), Salt Tectonics: A Global Perspective. AAPG Memoir, 65, pp. 77–108.

Gansser, A., 1960a. Die Geologische erforschung der Qom gegend. Iran. Bulletin der Vereinigung Schweitzerisches Petroleum Geologen und Ingenieur 23, 1–16.

Gansser, A., 1960b. Über Schlammvulkane und Salzdome. Naurforschende Gesellschaft in Zürich Vierteljahrschrift 105, 1–46.

Garcia Celma, A., Donker, H. (Eds.), 1996. The effect of gamma radiation in salt. EUR-Report 16743EN.

Gretener, P.E., 1982. Another look at the Alborz Nr. 5 in central Iran. Bulletin der Vereinigung Schweitzerisches Petroleum Geologen und Ingenieur 48, 1–8.

Handin, J., Russell, J.E., Carter, N.L., 1986. Experimental deformation of rocksalt. In: Hobbs, B.E., Heard, H.C. (Eds.), Mineral and Rock Deformation: Laboratory Studies. AGU Geophysical Monograph 36. American Geophysical Union, pp. 161–199.

Hansen, F.D., Carter, N.L., 1984. Creep of Avery Island rocksalt. In: Proceedings of the First Conference on Mechanical Behavior of Salt, Clausthal-Zellerfeld, Germany. Trans Tech Publications, pp. 53–69.

Hansen, F.D., Mellegard, K.D., 1980. Quasi-static strength and deformational characteristic of domal salt from Avery Island, Louisiana. ONWI-116, Report prepared by RE/SPEC Inc. for Office of Nuclear Waste Isolation.

Hickman, S.H., Evans, B., 1991. Experimental pressure solution in halite; the effect of grain/interphase boundary structure. Journal of the Geological Society 148, 549–560.

Horseman, S.T., Handin, J., 1990. Triaxial compression tests on rocksalt at temperatures from 50 °C to 200 °C and strain rates from 10^{-4} to 10^{-9} l/s. In: Duba, A.G., Durham, W.B., Handin, J.W., Wang, H.F. (Eds.), The Brittle–Ductile Transition in Rocks 56. American Geophysical Union, Washington, DC, pp. 103–110.

Horseman, S.T., Russell, J.E.H.J., Carter, N.L., 1992. Slow experimental deformation of Avery Island salt. In: Proceedings of the Seventh International Symposium on Salt, Kyoto, Japan, vol. 1, April 6–9, 1992. Elsevier, Amsterdam, pp. 67–74.

Humphreys, F.J., Hatherly, M., 1996. Recrystallization and Related Annealing Phenomena. Pergamon.

Hunsche, U., Schulze, O., Walter, F., Plischke, I., 2003. Projekt Gorleben. Thermomechanisches Verhalten von Salzgestein. 9G2138110000, BGR, Hannover.

Jackson, M.P.A., 1985. Natural Strain in Diapiric and Glacial Rock Salt, with Emphasis on Oakwood Dome, East Texas. Bureau of Economic Geology, The University of Texas at Austin, TX.

Jackson, M.P.A., Snelson, S., 1995. Retrospective salt tectonics. In: Jackson, M.P.A., Roberts, D.G. (Eds.), Salt Tectonics: A Global Perspective. AAPG Memoir 65, pp. 77–108.

Jackson, M.P.A., Cornelius, R.R., Craig, C.H., Gansser, A., Stocklin, J., Talbot, C.J., 1990. Salt Diapirs of the Great Kavir, Central Iran. Geological Society of America, Boulder 177.

Kupfer, D.H., 1974. Boundary shear zones in salt stocks. In: Fourth Symposium on Salt, Cleveland, Ohio, USA, 1, pp. 215–225.

Lohkämper, T.H.K., Jordan, G., Costamagna, R., Stöckhert, B., Schmahl, W.W., 2003. Phase shift interference microscope study of dissolution–precipitation processes of nonhydrostatically stressed halite crystals in solution. Contributions to Mineralogy and Petrology 146 (3), 263–274.

Lowenstein, T.K., Hardie, L.A., 1985. Criteria for the recognition of salt-pan evaporites. Sedimentology 32, 627–644.

Means, W.D., 1983. Microstructure and micromotion in recrystallization flow of octachloropropane: a first look. Geologische Rundschau 72 (2), 511–528.

Means, W.D., Ree, J.H., 1988. Seven types of subgrain boundaries in octachloropropane. Journal of Structural Geology 10, 765–770.

Mohr, M., Kukla, P.A., Urai, J.L., Bresser, G., 2005. Multiphase salt tectonic evolution in NW Germany: seismic interpretation and retrodefromation. International Journal of Earth Sciences 94 (5–6), 917–941.

Murata, K.J., Smith, R.L., 1946. Manganese and lead coactivators of red fluorescence in halite. American Mineralogist 31, 527–538.

Passchier, C.W., Trouw, R.A.J., 2005. Microtectonics. Springer.

Peach, C., Spiers, C.J., Trimby, P.W., 2001. Effect of confining pressure on dilatation, recrystallization, and flow of rock salt at 150 °C. Journal of Geophysical Research 106, 13315–13328.

Pennock, G.M., Drury, M.R., Spiers, C.J., 2005. The development of subgrain misorientations with strain in dry synthetic NaCl measured using EBSD. Journal of Structural Geology 27, 2159–2170.

Prior, D.J., Wheeler, J., Peruzzo, L., Spiess, R., Storey, C., 2002. Some garnet microstructures: an illustration of the potential of orientation maps and misorientation analysis in microstructural studies. Journal of Structural Geology 24 (6–7), 999–1011.

Przibram, K., 1954. Irradiation colours in minerals. Endeavour 13 (49), 37–41.

Ramsay, J., 1980. The crack-seal mechanism of rock deformation. Nature 284, 135–139.

Roedder, E., 1984. The fluids in salt. American Mineralogist 69, 413–439.

Rutter, E.H., Peach, C., White, S.H., Johnston, D., 1985. Experimental 'syntectonic' hydration of basalt. Journal of Structural Geology 7 (2), 251–266.

Schenk, O., Urai, J.L., 2004. Microstructural evolution and grain boundary structure during static recrystallization in synthetic polycrystals of sodium chloride containing saturated brine. Contributions to Mineralogy and Petrology 146 (6), 671–682.

Schléder, Z., Urai, J.L., 2005. Microstructural evolution of deformation-modified primary halite from the Middle Triassic Röt Formation at Hengelo, The Netherlands. International Journal of Earth Sciences 94 (5–6), 941–955.

Senseny, P.E., 1988. Creep properties of four salt rocks. In: Proceedings of the Second Conference on Mechanical Behavior of Salt, Clausthal-Zellerfeld, Germany. Trans Tech Publications, pp. 431–444.

Senseny, P.E., Hansen, F.D., Russell, J.E., Carter, N.L., Handin, J., 1992. Mechanical behaviour of rock salt: phenomenology and micromechanisms. International Journal of Rock Mechanics Mining Sciences. Geomechanical Abstracts 29 (4), 363–378.

Shearman, D.J., 1970. Recent halite rock, Baja California, Mexico. Transaction of Mining and Metallurgy 79B, 155–162.

Spiers, C.J., Carter, N.L., 1998. Microphysics of rocksalt flow in nature. In: Aubertin, M., Hardy, H.R. (Eds.), The Mechanical Behaviour of Salt: Proceedings of the Fourth Conference Series on Rock and Soil Mechanics. TTP Trans Tech Publications, Clausthal-Zellerfeld, vol. 22, pp. 115–128.

Spiers, C.J., Schutjens, P.M.T.M., Brezowski, R.H., Peach, C., Liezenberg, J.L., Zwart, H.J., 1990. Experimental determination of constitutive parameters governing creep of rocksalt by pressure solution. In: Knipe, R.J., Rutter, E.H. (Eds.), Deformation Mechanisms, Rheology and Tectonics. Geological Society, London, Special Publications, vol. 24, pp. 215–227.

Spiers, C.J., Urai, J.L., Lister, G.S., Boland, J.N., Zwart, H.J., 1986. The Influence of Fluid–Rock Interaction on the Rheology of Salt Rock. Department of Structural and Applied Geology, Institute of Earth Sciences. University of Utrecht, The Netherlands.

Talbot, C.J., 1979. Fold trains in a glacier of salt in southern Iran. Journal of Structural Geology 1 (1), 5–18.

Talbot, C.J., 1981. Sliding and other deformation mechanisms in glacier of salt, S Iran. In: McClay, K.R., Prince, N.J. (Eds.), Thrust and Nappe Tectonics. Geological Society, London, Special Publications, vol. 9, pp. 173–183.

Talbot, C.J., 1998. Extrusions of Hormuz salt in Iran. In: Blundell, D.J., Scott, A.C. (Eds.), Lyell; The Past is the Key to the Present. Geological Society, London, Special Publications, vol. 143, pp. 315–334.

Talbot, C.J., in preparation. The Eyvanekey plateau, a 20 × 10 km sheet of allochtonous salt near Garmsar.

Talbot, C.J., Aftabi, P., 2004. Geology and models of salt extrusion at Qom Kuh, central Iran. Journal of the Geological Society 161, 321–334.

Talbot, C.J., Jarvis, R.J., 1984. Age, budget and dynamics of an active salt extrusion in Iran. Journal of Structural Geology 6 (5), 521–533.

Talbot, C.J., Medvedev, S., Alavi, M., Shahrivar, H., Heidari, E., 2000. Salt extrusion at Kuh-e-Jahani, Iran, from June 1994 to November 1997. In: Vendeville, B.C., Mart, Y., Vigneresse, J.-L. (Eds.), Salt, Shale and Igneous Diapirs in and around Europe. Geological Society, London, Special Publications, vol. 174, pp. 93–110.

Talbot, C.J., Rogers, E.A., 1980. Seasonal movements in a salt glacier in Iran. Science 208, 395–397.

Ter Heege, J.H., De Bresser, J.H.P., Spiers, C.J., 2005a. Dynamic recrystallization of wet synthetic polycrystalline halite: dependence of grain size distribution on flow stress, temperature and strain. Tectonophysics 396, 35–57.

Ter Heege, J.H., De Bresser, J.H.P., Spiers, C.J., 2005b. Rheological behaviour of synthetic rocksalt: the interplay between water, dynamic recrystallization and deformation mechanisms. Journal of Structural Geology 27 (6), 948–963.

Twiss, R.J., 1977. Theory and applicability of a recrystallized grain size paleopiezometer. Pageoph 115, 227–244.

Urai, J.L., Spiers, C.J., Peach, C., Franssen, R.C.M.W., Liezenberg, J.L., 1987. Deformation mechanisms operating in naturally deformed halite rocks as deduced from microstructural investigations. Geologie en Mijnbouw 66, 165–176.

Urai, J.L., Spiers, C.J., Peach, C.J., Zwart, H.J., 1985. A laboratory investigation into the interaction of recrystallization and radiation damage effects in polycrystalline salt rocks. HPT Laboratorium, Insititut voor Aardwetenschappen, University of Utrecht, The Netherlands.

Urai, J.L., Spiers, C.J., Zwart, H.J., Lister, G.S., 1986. Weakening of rocksalt by water during long term creep. Nature 324, 554–557.

van Opbroek, G., den Hartog, H.W., 1985. Radiation damage of NaCl: dose rate effects. Journal of Physics C: Solid State Physics 18, 257–268.

Volozh, Y., Talbot, C.J., Ismail-Zadeh, A., 2003. Salt structures and hydrocarbons in the Pricaspian basin. AAPG Bulletin 87 (2), 313–334.

Warren, J., 2006. Evaporites: Sediments, Resources and Hydrocarbons. Springer.

Watanabe, T., Peach, C., 2002. Electrical impedance measurement of plastically deforming halite rocks at 125 °C and 50 MPa. Journal of Geophysical Research 107 (B1), ECV 2-1–ECV 2-12.

Wawersik, W.R., Zeuch, D.H., 1986. Modeling and mechanistic interpretation of creep of rock salt below 200 °C. Tectonophysics 121, 125–152.

Wenkert, D.D., 1979. The flow of salt glaciers. Geophysical Research Letters 6 (6), 523–525.

Wheeler, J., Prior, D.J., Jiang, Z., Spiess, R., Trimby, P.W., 2001. The petrological significance of misorientation between grains. Contributions to Mineralogy and Petrology 141, 109–124.